

# Calculations of Polarization Observables in Pseudoscalar Meson Photo-production Reactions

A. M. Sandorfi,<sup>1,\*</sup> S. Hoblit,<sup>2</sup> H. Kamano,<sup>1</sup> and T.-S. H. Lee<sup>3,1</sup>

<sup>1</sup>*Thomas Jefferson National Accelerator Facility,  
Newport News, Virginia 23606, USA*

<sup>2</sup>*Department of Physics, University of Virginia,  
Charlottesville, Virginia 22901, USA*

<sup>3</sup>*Physics Division, Argonne National Laboratory, Illinois 60439, USA*

(Dated: November 15, 2018)

## Abstract

In preparation for the extraction of pseudoscalar meson photo-production amplitudes from a new generation of complete experiments, we assemble the relations between experimental observables and the Chew-Goldberger-Low-Nambu amplitudes. We present expressions that allow the direct calculation of matrix elements with arbitrary spin projections and uses these to clarify sign differences that exist in the literature. Comparing to the MAID and SAID analysis codes, we have found that the implied definitions of six double-polarization observables are the negative of what has been used in comparing to recent experimental data.

PACS numbers: 13.60.Le, 13.75.Gx, 13.75.Jz

---

\*Corresponding author: sandorfi@jlab.org

## I. INTRODUCTION

As a consequence of dynamic chiral symmetry breaking, the Goldstone bosons ( $\pi, \eta, K$ ) dress the nucleon and alter its spectrum. Not surprisingly, pseudoscalar meson production has been a powerful tool in studying the spectrum of excited nucleon states. However, such states are short lived and broad so that above the energy of the first resonance, the  $P_{33}\Delta(1232)$ , the excitation spectrum is a complicated overlap of many resonances. Isolating any one and separating it from backgrounds has been a long-standing problem in the literature.

The spin degrees of freedom in meson photo-production provide signatures of interfering partial wave strength that are often dramatic and have been useful for differentiating between models of meson production amplitudes. Models that must account for interfering resonance amplitudes and non-resonant contributions are often severely challenged by new polarization data. Ideally, one would like to partition the problem by first determining the amplitudes from experiment, at least to within a phase, and then relying upon a model to separate resonances from non-resonant processes. Single-pseudoscalar photo-production is described by 4 complex amplitudes (two for the spin states of the photon, two for the nucleon target and two for the baryon recoil, which parity considerations reduces to a total of 4). To avoid ambiguities, it was shown[1] that angular distribution measurements of at least 8 carefully chosen observables at each energy for both proton and neutron targets must be performed. While such experimental information has not yet been available, even after 50 years of photo-production experiments, a sequence of *complete* experiments are now underway at Jefferson Lab [2, 3], as well as complementary experiments at the electron facilities in Bonn and Mainz, with the goal of obtaining a direct determination of the amplitude to within a phase, for at least a few production channels, notably  $K\Lambda$  and possibly  $\pi N$ .

Our purpose here is to assemble the relations between experimental observables and the Chew-Goldberger-Low-Nambu (CGLN) amplitudes [4], and to clarify sign differences that exist in the literature. The four CGLN amplitudes can be expressed in Cartesian ( $F_i$ ), Spherical or Helicity ( $H_i$ ), or Transversity ( $b_i$ ) representations. While the latter two choices afford some theoretical simplifications when predicting asymmetries from model amplitudes [5], when working in the reverse direction, fitting asymmetries to extract amplitudes, such simplifications are largely moot. In practice, one expands the amplitudes in multipoles and

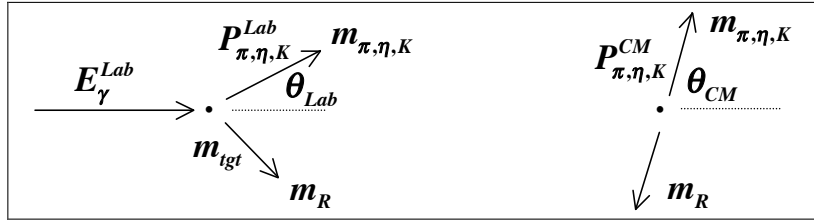


FIG. 1: Kinematic variables in meson photo-production in Lab and CM frames.

fits the multipoles directly. This both facilitates the search for resonance behavior and allows the use of full angular distribution data at a fixed energy to constrain angle-independent quantities. (Extracting the four CGLN amplitudes directly would require separate fits at each angle, along with some way of constraining an arbitrary phase which could be angle dependent.) Here we restrict our considerations to the CGLN  $F_i$  representation, which has the simplest decomposition into multipoles [4], Eqs. (17)-(20) below.

In single-pseudoscalar meson photo-production there are 16 possible observables, the cross section ( $\sigma$ ), three single polarization asymmetries determined by the beam, target or recoil polarizations ( $\Sigma, T, P$ ), and three sets of four asymmetries that depend on the polarization combinations of beam-target (BT), beam-recoil (BR) and target-recoil (TR), as in [5]. Expressions for at least some of these observables in terms of the CGLN  $F_i$  appear already in earlier papers [6, 7]. The available complete expressions can be classified into two groups [8, 9] and [10, 11]. In all cases we have found in the literature, the magnitudes of the expressions relating the CGLN  $F_i$  to experimental observables are identical, but the signs of some appear to differ. In particular, sign differences have occurred in double-polarization observables for which little data have been available until very recently. There is also a set of 37 *Fierz* identities interrelating the 16 polarization observables, the most complete list being given in [1]. We have found many of the signs in the expressions of this list to be incompatible with either group of papers, [8, 9] or [10, 11].

In sections II and III, we give explicit and complete formulae that allow the direct numerical calculation of matrix elements with arbitrary spin projections, which are then used to evaluate polarization observables from the four CGLN  $F_i$  amplitudes. In so doing, we resolve the previous sign ambiguities and collect a complete set of expressions that can be used to extract multipole amplitudes from the new set of *complete* experiments that are now underway. This is discussed in section IV with a brief summary. To avoid possible

mis-interpretation of the signs of the formulae presented in this paper, the directions of the polarization vectors for all 16 observables are given explicitly in Appendix A. The Fierz realtions with consistent signs are given in Appendix B.

## II. KINEMATICS AND COORDINATE DEFINITIONS

The kinematic variables of meson photo-production used in our derivations are specified in Fig. 1. Some useful relations are :

- The total center of mass (CM) energy:

$$W = \sqrt{s} = \sqrt{m_{\text{tgt}}(m_{\text{tgt}} + 2E_{\gamma}^{\text{Lab}})}. \quad (1)$$

- The laboratory (Lab) energy needed to excite the hadronic system with total CM energy  $W$ :

$$E_{\gamma}^{\text{Lab}} = \frac{W^2 - m_{\text{tgt}}^2}{2m_{\text{tgt}}}. \quad (2)$$

- The energy of the photon in the CM frame:

$$E_{\gamma}^{\text{CM}} = \frac{W^2 - m_{\text{tgt}}^2}{2W} = q. \quad (3)$$

- The magnitude of the 3-momentum of the meson in the CM frame:

$$|P_{\pi,\eta,K}^{\text{CM}}| = \frac{W}{2} \left\{ \left[ 1 - \left( \frac{m_{\pi,\eta,K} + m_R}{W} \right)^2 \right] \left[ 1 - \left( \frac{m_{\pi,\eta,K} - m_R}{W} \right)^2 \right] \right\}^{1/2} = k. \quad (4)$$

- The density of state factor:

$$\rho = |P_{\pi,\eta,K}^{\text{CM}}| / E_{\gamma}^{\text{cm}}. \quad (5)$$

The definitions of Polarization angles used in our derivation are shown in Fig. 2 for the case of  $K \Lambda$  production. The  $\langle \hat{x} - \hat{z} \rangle$  plane is the reaction plane in the center of mass. The figure illustrates the case of linear  $\gamma$  polarization, with the alignment vector  $P_L^{\gamma}$  (parallel to the oscillating electric field of the photon) in the  $\langle \hat{x} - \hat{y} \rangle$  plane at  $\phi_{\gamma}$ , rotating clockwise from  $\hat{x}$  towards  $\hat{y}$ . The target nucleon polarization  $\vec{P}^T$  is specified by polar angle  $\theta_p$  measured from  $\hat{z}$ , and azimuthal angle  $\phi_p$  in the  $\langle \hat{x} - \hat{y} \rangle$  plane, rotating clockwise from  $\hat{x}$  towards  $\hat{y}$ . The recoil  $\Lambda$  is in the  $\langle \hat{x} - \hat{z} \rangle$  plane; its polarization  $\vec{P}_{\Lambda}^R$  is at polar  $\theta_{p'}$ , measured from  $\hat{z}$ , and azimuthal  $\phi_{p'}$  in the  $\langle \hat{x} - \hat{y} \rangle$  plane, rotating clockwise from  $\hat{x}$  to  $\hat{y}$ .

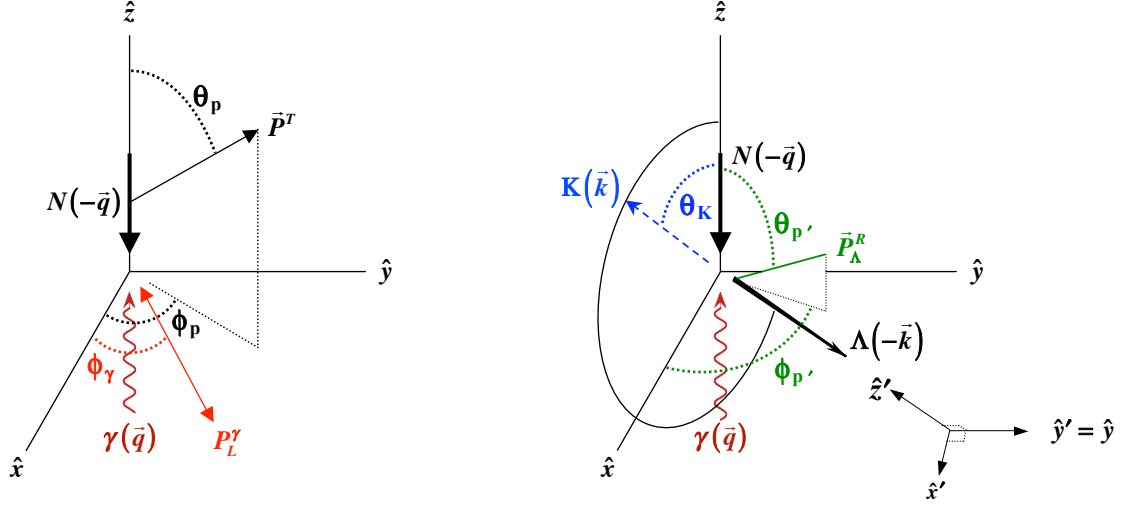


FIG. 2: The CM coordinate system and angles used to specify polarizations in the reaction,  $\gamma(\vec{q}, \vec{P}^\gamma) + N(-\vec{q}, \vec{P}^T) \rightarrow K(\vec{k}) + \Lambda(-\vec{k}, \vec{P}_\Lambda^R)$ . The left (right) side is for the initial  $\gamma N$  (final  $K\Lambda$ ) system.

The case of circular photon polarization can potentially lead to some confusion. Most particle physics literature designates circular states as  $r$ , for right circular (or  $l$ , for left circular), referring to the fact that with  $r$  polarization the electric vector of the photon appears to rotate clockwise *when the photon is traveling away from the observer*. However, when the same photon is viewed by an observer facing the incoming photon the electric vector appears to rotate counter-clockwise. For this reason optics literature traditionally designates this same state as  $l$  circularly polarized. Nonetheless, both conventions agree on the value of the photon helicity [12]  $h = \vec{S} \cdot \vec{P} / |\vec{P}| = \pm 1$  and so we use only the helicity designations here,  $\vec{P}_c^\gamma = +1(-1)$  when 100% of the photon spins are parallel (anti-parallel) to the photon momentum vector.

In terms of these polarization vectors, the general form of the cross section is written as,

$$\begin{aligned}
d\sigma = & \frac{1}{2} \left( d\sigma_0 + \hat{\Sigma}[-P_L^\gamma \cos(2\phi_\gamma)] + \hat{T}[P_y^T] + \hat{P}[P_{y'}^R] \right. \\
& + \hat{E}[-P_c^\gamma P_z^T] + \hat{G}[P_L^\gamma P_z^T \sin(2\phi_\gamma)] + \hat{F}[P_c^\gamma P_x^T] + \hat{H}[P_L^\gamma P_x^T \sin(2\phi_\gamma)] \\
& + \hat{C}_{x'}[P_c^\gamma P_{x'}^R] + \hat{C}_{z'}[P_c^\gamma P_{z'}^R] + \hat{O}_{x'}[P_L^\gamma P_{x'}^R \sin(2\phi_\gamma)] + \hat{O}_{z'}[P_L^\gamma P_{z'}^R \sin(2\phi_\gamma)] \\
& \left. + \hat{L}_{x'}[P_z^T P_{x'}^R] + \hat{L}_{z'}[P_z^T P_{z'}^R] + \hat{T}_{x'}[P_x^T P_{x'}^R] + \hat{T}_{z'}[P_x^T P_{z'}^R] \right). \quad (6)
\end{aligned}$$

Here  $\sigma_0$  is the cross section averaged over all initial state polarizations, and summed over final state polarization. We have designated the product of an asymmetry and  $\sigma_0$  with a caret, so that  $\hat{A} = A\sigma_0$ . (These products are referred to as *profile functions* in ref. [1, 9].) The terms in this expression contain the single polarization, BT, BR and TR observables. Two terms here have negative coefficients. The first arises because we have taken for the numerator of the beam asymmetry ( $\Sigma$ ) the somewhat more common definition of  $(\sigma_{\perp} - \sigma_{\parallel})$ , rather than the other way around. (Here  $\perp$  ( $\parallel$ ) corresponds to  $\vec{P}_{\gamma}^L = \hat{y}(\hat{x})$  in the left panel of Fig. 2.) For the second, because of its connection to sum rules the numerator of the  $E$  asymmetry is almost always defined in terms of the total CM entrance channel helicity,  $(\sigma_{3/2} - \sigma_{1/2})$ , and these correspond to anti-parallel and parallel photon and target spin alignments, respectively. The specific measurements needed to construct each of these observables is tabulated in Appendix A. (The above expression contains only the leading polarization terms. Each single polarization observable has another higher order term that depends on two polarization quantities, and each double has another term dependent on three polarizations. For simplicity, we defer these to a later discussion.)

Recoil observables are generally specified in the rotated coordinate system with  $\hat{z}' = +\vec{k}$  (*opposite* to the recoil  $\Lambda$  momentum);  $\hat{y}' = \hat{y}$  and  $\hat{x}' = \hat{y}' \times \hat{z}' = \hat{y} \times \vec{k}$ . Occasionally, a particular recoil observable will have a more transparent interpretation in the unprimed coordinate system of Fig. 2 [13]. Since a baryon polarization transforms as a standard three vector, the *unprimed* and *primed* observables are simply related:

$$A_x = +A_{x'} \cos \theta_K + A_{z'} \sin \theta_K, \quad (7)$$

$$A_z = -A_{x'} \sin \theta_K + A_{z'} \cos \theta_K, \quad (8)$$

where  $A$  represents any one of the BR or TR observables.

### III. CALCULATION OF POLARIZATION OBSERVABLES

With the variables specified in Fig. 2, the differential cross section of  $\gamma(\vec{q}, P^{\gamma}) + N(-\vec{q}, m_{s_N}) \rightarrow K(\vec{k}) + \Lambda(-\vec{k}, m_{s_{\Lambda}})$  in the center of mass frame can be written as

$$\frac{d\sigma}{d\Omega}(m_{s_{\Lambda}}; P^{\gamma}, m_{s_N}) = \frac{1}{(4\pi)^2} \frac{k m_N m_{\Lambda}}{q W^2} |\bar{u}_{\Lambda}(-\vec{k}, m_{s_{\Lambda}}) I^{\mu} \epsilon_{\mu}(q, P^{\gamma}) u_N(-\vec{q}, m_{s_N})|^2, \quad (9)$$

where  $W = q + E_N(q) = E_K(k) + E_{\Lambda}(k)$ ;  $\epsilon_{\mu}(q, P^{\gamma})$  is the photon polarization vector;  $m_{s_{\Lambda}}$ , and  $m_{s_N}$  are the spin quantum number of the  $\Lambda$  and the nucleon in the z-direction, respectively;

$\bar{u}_\Lambda I^\mu \epsilon_\mu u_N$  is normalized to the usual invariant amplitude calculated from a Lagrangian in the convention of Bjorken and Drell [14]. The CGLN amplitude is defined by

$$\bar{u}_\Lambda(-\vec{k}, m_{s_\Lambda}) I^\mu \epsilon_\mu(q, P^\gamma) u_N(-\vec{q}, m_{s_N}) = -\frac{4\pi W}{\sqrt{m_N m_\Lambda}} \chi_{m_{s_\Lambda}}^+ F_{CGLN} \chi_{m_{s_N}}, \quad (10)$$

where  $\chi_{m_s}$  is the usual eigenstate of the Pauli operator  $\sigma_z$ , and

$$F_{CGLN} = \sum_{i=1,4} O_i F_i(\theta_K, E), \quad (11)$$

with

$$O_1 = -i\vec{\sigma} \cdot \vec{P}^\gamma, \quad (12)$$

$$O_2 = -[\vec{\sigma} \cdot \hat{k}][\vec{\sigma} \cdot (\hat{q} \times \vec{P}^\gamma)], \quad (13)$$

$$O_3 = -i[\vec{\sigma} \cdot \hat{q}][\hat{k} \cdot \vec{P}^\gamma], \quad (14)$$

$$O_4 = -i[\vec{\sigma} \cdot \hat{k}][\hat{k} \cdot \vec{P}^\gamma], \quad (15)$$

where  $\hat{p} = \vec{p}/|\vec{p}|$ . We then obtain

$$\frac{d\sigma}{d\Omega}(m_{s_\Lambda}; P^\gamma, m_{s_N}) = \frac{k}{q} |\chi_{m_{s_\Lambda}}^+ F_{CGLN} \chi_{m_{s_N}}|^2. \quad (16)$$

The formula for calculating CGLN amplitudes from multipoles are well known [4] and are given below:

$$F_1 = \sum_{l=0}^{l_{max}} [P'_{l+1}(x)E_{l+} + P'_{l-1}(x)E_{l-} + lP'_{l+1}(x)M_{l+} + (l+1)P'_{l-1}(x)M_{l-}], \quad (17)$$

$$F_2 = \sum_{l=0}^{l_{max}} [(l+1)P'_l(x)M_{l+} + lP'_l(x)M_{l-}], \quad (18)$$

$$F_3 = \sum_{l=0}^{l_{max}} [P''_{l+1}(x)E_{l+} + P''_{l-1}(x)E_{l-} - P''_{l+1}(x)M_{l+} + P''_{l-1}(x)M_{l-}], \quad (19)$$

$$F_4 = \sum_{l=0}^{l_{max}} [-P''_l(x)E_{l+} - P''_l(x)E_{l-} + P''_l(x)M_{l+} - P''_l(x)M_{l-}]. \quad (20)$$

where  $x = \hat{k} \cdot \hat{q} = \cos\theta_K$ ,  $l$  is the orbital angular momentum of the  $K\Lambda$  system, and  $P'_l(x) = dP_l(x)/dx$  and  $P''_l(x) = d^2P_l(x)/dx^2$  are the derivatives of the Legendre function  $P_l(x)$ , with the understanding that  $P'_{-1} = P''_{-1} = 0$ . The value of  $l_{max}$  depends obviously on the energy.

In order to calculate the 16 polarization observables in accordance with the experimental geometry defined in Appendix A, we need a formula for calculating cross sections with arbitrary spin projections for the initial and final baryon states,  $\gamma(\vec{q}, \vec{P}^\gamma) + N(-\vec{q}, \vec{P}^T) \rightarrow K(\vec{k}) + \Lambda(-\vec{k}, \vec{P}^R)$ , specified in Fig. 2. Here linear photon polarization must be in the  $\langle \hat{x} - \hat{y} \rangle$  plane, but  $\vec{P}^T$  and  $\vec{P}^R$  can be in any directions. Such cross section formula can be obtained by simply replacing  $|\chi_{m_s\Lambda}^+ F_{CGLN} \chi_{m_sN}|^2$  in Eq. (16) by  $|\langle \lambda_{\vec{P}^R} | F_{CGLN} | \lambda_{\vec{P}^T} \rangle|^2$ :

$$\frac{d\sigma}{d\Omega}(\vec{P}^\gamma, \vec{P}^T, \vec{P}^R) = \frac{k}{q} |\langle \lambda_{\vec{P}^R} | F_{CGLN} | \lambda_{\vec{P}^T} \rangle|^2, \quad (21)$$

where  $|\lambda_{\vec{P}^T}\rangle$  ( $\langle \lambda_{\vec{P}^R}|$ ) is a helicity state of the initial (final) baryon moving in the  $\vec{P}^T$  ( $\vec{P}^R$ ) direction. The helicity state in the direction of an arbitrary vector  $\vec{p} = (p, \theta_p, \phi_p)$  is defined by

$$\vec{S} \cdot \hat{p} |\lambda_{\vec{p}}\rangle = \lambda_{\vec{p}} |\lambda_{\vec{p}}\rangle, \quad (22)$$

where  $\vec{S}$  is the spin operator. For the spin 1/2 particles,  $\vec{S}$  is expressed with the Pauli matrix:  $\vec{S} = \vec{\sigma}/2$ .

Our next task is to derive explicit formulae for calculating the matrix element  $\langle \lambda_{\vec{P}^R} | F_{CGLN} | \lambda_{\vec{P}^T} \rangle$  in terms of the CGLN amplitudes  $F_i$  in Eqs. (17)-(20). It is known that the helicity state is related to the usual eigenstate of z-axis quantization by rotations:

$$|\lambda_{\vec{p}}\rangle = \sum_{m_s=\pm 1/2} D_{m_s, \lambda_{\vec{p}}}^{(1/2)}(\phi_p, \theta_p, -\phi_p) |m_s\rangle, \quad (23)$$

where  $|m_s\rangle$  is defined as  $S_z |\pm 1/2\rangle = (\pm 1/2) |\pm 1/2\rangle$ , and

$$D_{m_s, \lambda_{\vec{p}}}^{(1/2)}(\phi_p, \theta_p, -\phi_p) = e^{-i(m_s - \lambda_{\vec{p}})\phi_p} d_{m_s, \lambda_{\vec{p}}}^{1/2}(\theta_p). \quad (24)$$

We recall

$$\begin{aligned} d_{1/2, 1/2}^{1/2}(\theta) &= d_{-1/2, -1/2}^{1/2}(\theta) = \cos \frac{\theta}{2}, \\ d_{-1/2, 1/2}^{1/2}(\theta) &= -d_{1/2, -1/2}^{1/2}(\theta) = \sin \frac{\theta}{2}. \end{aligned} \quad (25)$$

Equation (23) can be easily verified by explicit calculations using the definition (22) and properties (24) and (25) for the special cases where  $\hat{p} = \hat{x}, \hat{y}, \hat{z}$  and the usual definition of the Pauli matrices,  $(\sigma_i)_{mm'}$  ( $i = x, y, z$  and  $m$  (row),  $m'$  (column) =  $+1/2, -1/2$ ),

$$\sigma_x = \begin{pmatrix} 0 & 1 \\ 1 & 0 \end{pmatrix}, \quad \sigma_y = \begin{pmatrix} 0 & -i \\ i & 0 \end{pmatrix}, \quad \sigma_z = \begin{pmatrix} 1 & 0 \\ 0 & -1 \end{pmatrix}. \quad (26)$$

TABLE I:  $C_{i,n}(\theta_K, \phi_\gamma)$  of Eqs. (33) and (35)

	$n = 0$	$n = 1$	$n = 2$	$n = 3$
$i = 1$	0	$-i \cos \phi_\gamma$	$-i \sin \phi_\gamma$	0
$i = 2$	$\sin \theta_K \sin \phi_\gamma$	$i \cos \theta_K \cos \phi_\gamma$	$i \cos \theta_K \sin \phi_\gamma$	$-i \sin \theta_K \cos \phi_\gamma$
$i = 3$	0	0	0	$-i \sin \theta_K \cos \phi_\gamma$
$i = 4$	0	$-i \sin^2 \theta_K \cos \phi_\gamma$	0	$-i \sin \theta_K \cos \theta_K \cos \phi_\gamma$

From Fig. 2, the momenta and linear photon polarization are expressed as

$$\vec{q} = q(0, 0, 1), \quad (27)$$

$$\vec{k} = k(\sin \theta_K, 0, \cos \theta_K), \quad (28)$$

$$\vec{P}^\gamma = (\cos \phi_\gamma, \sin \phi_\gamma, 0). \quad (29)$$

Circular photon polarizations of helicity  $\lambda_\gamma$  are expressed in terms of linear polarizations as

$$(P_c^\gamma)_{\lambda_\gamma=\pm 1} = \mp \frac{1}{\sqrt{2}}(P_x^\gamma \pm iP_y^\gamma). \quad (30)$$

For the initial and final baryon polarizations, we use the spherical variables:

$$\vec{P}^T = (1, \theta_p, \phi_p), \quad (31)$$

$$\vec{P}^R = (1, \theta_{p'}, \phi_{p'}). \quad (32)$$

By using Eqs. (27)-(29), we can rewrite  $O_i$  in Eq. (11) as

$$O_i = \sum_{n=0,3} C_{i,n}(\theta_K, \phi_\gamma) \sigma_n, \quad (33)$$

where  $\sigma_0 = 1$ ,  $\sigma_1 = \sigma_x$ ,  $\sigma_2 = \sigma_y$ ,  $\sigma_3 = \sigma_z$ . The explicit form of  $C_{i,n}$  is shown in Table I.

By using Eq. (23) and Eqs. (11) and (33), the photo-production matrix element can then be calculated from

$$\langle \lambda_{\hat{P}R} | F_{\text{CGLN}} | \lambda_{\hat{P}T} \rangle = \sum_{n=0,3} G_n(\theta_K, \phi_\gamma) \langle \lambda_{\hat{P}R} | \sigma_n | \lambda_{\hat{P}T} \rangle, \quad (34)$$

with

$$G_n(\theta_K, \phi_\gamma) = \sum_{i=1,4} F_i(\theta_K, E) C_{i,n}(\theta_K, \phi_\gamma), \quad (35)$$

$$\langle \lambda_{\hat{P}R} | \sigma_n | \lambda_{\hat{P}T} \rangle = \sum_{m_{s'}, m_s = \pm 1/2} D_{m_{s'}, \lambda_{\hat{P}R}}^{(1/2)*}(\phi_{p'}, \theta_{p'}, -\phi_{p'}) D_{m_s, \lambda_{\hat{P}T}}^{(1/2)}(\phi_p, \theta_p, -\phi_p) \langle m_{s'} | \sigma_n | m_s \rangle, \quad (36)$$

where  $\langle m'_s | \sigma_n | m_s \rangle = (\sigma_n)_{m'_s, m_s}$  can be calculated from Eq. (26).

We may now generate multipoles from a model and then use Eqs. (17)-(20) to calculate the CGLN amplitudes, which are then used to calculate the matrix element  $\langle \lambda_{\vec{p}R} | F_{CGLN} | \lambda_{\vec{p}T} \rangle$  by using Eqs. (34)-(36). Equation (21) then allows us to calculate all possible polarization observables.

#### IV. RELATING OBSERVABLES TO CGLN AMPLITUDES

We are now in a position to use any set of multipole amplitudes to calculate CGLN amplitudes by using Eqs. (17)-(20), and then use these to evaluate: (a) the polarization observables by using the formulae described in the previous section and the spin projections specified in the table in the Appendix A, and (b) the same observables calculated from the analytic expressions, as given in [8, 9] or [10, 11]. As expected, the absolute magnitudes from two methods are the same, but some of their signs are different. In doing so, we are able to fix the signs of the analytic expressions for the experimental conditions specified in Fig. 2 and Appendix A. Our results are:

$$\begin{aligned} \sigma_0 = & +\Re e \{ F_1^* F_1 + F_2^* F_2 + \sin^2 \theta (F_3^* F_3 / 2 + F_4^* F_4 / 2 + F_2^* F_3 + F_1^* F_4 \\ & + \cos \theta F_3^* F_4) - 2 \cos \theta F_1^* F_2 \} \rho \end{aligned} \quad (37a)$$

$$\hat{\Sigma} = -\sin^2 \theta \Re e \{ (F_3^* F_3 + F_4^* F_4) / 2 + F_2^* F_3 + F_1^* F_4 + \cos \theta F_3^* F_4 \} \rho \quad (37b)$$

$$\hat{T} = +\sin \theta \Im m \{ F_1^* F_3 - F_2^* F_4 + \cos \theta (F_1^* F_4 - F_2^* F_3) - \sin^2 \theta F_3^* F_4 \} \rho \quad (37c)$$

$$\hat{P} = -\sin \theta \Im m \{ 2F_1^* F_2 + F_1^* F_3 - F_2^* F_4 - \cos \theta (F_2^* F_3 - F_1^* F_4) - \sin^2 \theta F_3^* F_4 \} \rho \quad (37d)$$

$$\hat{E} = +\Re e \{ F_1^* F_1 + F_2^* F_2 - 2 \cos \theta F_1^* F_2 + \sin^2 \theta (F_2^* F_3 + F_1^* F_4) \} \rho \quad (37e)$$

$$\hat{G} = +\sin^2 \theta \Im m \{ F_2^* F_3 + F_1^* F_4 \} \rho \quad (37f)$$

$$\hat{F} = +\sin \theta \Re e \{ F_1^* F_3 - F_2^* F_4 - \cos \theta (F_2^* F_3 - F_1^* F_4) \} \rho \quad (37g)$$

$$\hat{H} = -\sin \theta \Im m \{ 2F_1^* F_2 + F_1^* F_3 - F_2^* F_4 + \cos \theta (F_1^* F_4 - F_2^* F_3) \} \rho \quad (37h)$$

$$\hat{C}_{x'} = -\sin \theta \Re e \{ F_1^* F_1 - F_2^* F_2 - F_2^* F_3 + F_1^* F_4 - \cos \theta (F_2^* F_4 - F_1^* F_3) \} \rho \quad (37i)$$

$$\hat{C}_{z'} = -\Re e \{ 2F_1^* F_2 - \cos \theta (F_1^* F_1 + F_2^* F_2) + \sin^2 \theta (F_1^* F_3 + F_2^* F_4) \} \rho \quad (37j)$$

$$\hat{O}_{x'} = -\sin \theta \Im m \{ F_2^* F_3 - F_1^* F_4 + \cos \theta (F_2^* F_4 - F_1^* F_3) \} \rho \quad (37k)$$

$$\hat{O}_{z'} = +\sin^2 \theta \Im m \{ F_1^* F_3 + F_2^* F_4 \} \rho \quad (37l)$$

$$\begin{aligned}\hat{L}_{x'} &= +\sin\theta\Re\{F_1^*F_1 - F_2^*F_2 - F_2^*F_3 + F_1^*F_4 + \sin^2\theta(F_4^*F_4 - F_3^*F_3)/2 \\ &\quad + \cos\theta(F_1^*F_3 - F_2^*F_4)\}\rho\end{aligned}\quad (37m)$$

$$\begin{aligned}\hat{L}_{z'} &= +\Re\{2F_1^*F_2 - \cos\theta(F_1^*F_1 + F_2^*F_2) + \sin^2\theta(F_1^*F_3 + F_2^*F_4 + F_3^*F_4) \\ &\quad + \cos\theta\sin^2\theta(F_3^*F_3 + F_4^*F_4)/2\}\rho\end{aligned}\quad (37n)$$

$$\hat{T}_{x'} = -\sin^2\theta\Re\{F_1^*F_3 + F_2^*F_4 + F_3^*F_4 + \cos\theta(F_3^*F_3 + F_4^*F_4)/2\}\rho\quad (37o)$$

$$\begin{aligned}\hat{T}_{z'} &= +\sin\theta\Re\{F_1^*F_4 - F_2^*F_3 + \cos\theta(F_1^*F_3 - F_2^*F_4) \\ &\quad + \sin^2\theta(F_4^*F_4 - F_3^*F_3)/2\}\rho\end{aligned}\quad (37p)$$

A comparable set of expressions are given by Fasano, Tabakin and Saghai (FTS) in [9]. That paper defines the photon polarization using Stokes vectors taken from optics where right and left circular polarization are interpreted differently. Nonetheless, they associate photon helicity +1 with what Ref. [9] refers to as  $r$  circular polarization. Keeping this convention and allowing for their different definition of the  $E$  beam-target asymmetry, the above expressions are consistent with those of [9].

Comparing the above relations to those given by Knöchlein, Drechsel and Tiator (KDT) (Appendix B and C of [11]), six have different signs, the BT observable  $H$ , the TR observable  $L_{x'}$  and all four of the BR observables  $C_{x'}$ ,  $C_{z'}$ ,  $O_{x'}$  and  $O_{z'}$ . The KDT paper of [11] is listed in the MAID on-line meson production analysis [15–17] as the defining reference for the connection between CGLN amplitudes and polarization observables. To check if these differences persist in the MAID code we have downloaded MAID multipoles, used the relations in Eqs. (17)-(20) to construct from these the four CGLN  $F_i$  amplitudes, and then used our equations (37) above to construct observables. Comparing the results to direct predictions of observables from the MAID code, we find the same six sign differences. However, in the general form of the cross section given by KDT in [11] these six observables appear with a negative coefficient, as opposed to our form of the cross section in Eq. (6). This is equivalent to interchanging the  $\sigma_1$  and  $\sigma_2$  measurements of Appendix A that are needed to construct these six observables. The choice of these two measurements that we list in Appendix A seem the obvious ones. They are, with the exception of the  $E$  asymmetry, the same choices used by FTS in [9]. Despite the fact that KDT refer to their definition of observables as *common* to FTS in [9], there is evidently a sign difference for  $H$ ,  $L_{x'}$ ,  $C_{x'}$ ,  $C_{z'}$ ,  $O_{x'}$  and  $O_{z'}$ .

We have conducted a similar test with the GWU/VPI SAID on-line analysis code [18, 19], downloading SAID multipoles, using the relations in Eqs. (17)-(20) to construct from these the four CGLN  $F_i$  amplitudes, and then using our equations (37) above to construct observables. When the results are compared to direct predictions of observables from the SAID code, again the same 6 observables ( $H, L_{x'}, C_{x'}, C_{z'}, O_{x'}, O_{z'}$ ) differ in sign. For the definition of observables, SAID refers to the Barker, Donnachie and Storrow paper of [5]. That paper is in general too condensed to definitively address signs, but at least in the case of  $O_{x'}$  they define the required (B,T,R) measurements as  $(\pm\pi/4, -, x')$  which is in agreement with our choice in Appendix A.

New data are emerging from the current generation of polarization experiments which make these sign differences an important issue. In Ref. [13], recent results for the  $C_{x'}$  and  $C_{z'}$  asymmetries have been compared with the direct predictions of the Kaon-MAID code, ignoring the sign reversal. This has particularly dramatic consequences for the BR asymmetry  $C_{z'}$  which is constrained by angular momentum conservation to the value of +1 at 0 degrees. This is straightforward to see from Appendix A, where  $C_{z'} = \{\sigma_1(+1, 0, +z') - \sigma_2(+1, 0, -z')\}/\{\sigma_1 + \sigma_2\}$ . When the incident photon spin is oriented along  $+\hat{z}$ , only those target nucleons with anti-parallel spin can contribute to the production of spin zero mesons at 0 degrees, and the projection of the total angular momentum along  $\hat{z}$  is  $+\frac{1}{2}$ . Thus, the recoil baryon must have its spin oriented along  $+\hat{z} = +\hat{z}'$ , so that  $\sigma_2$  must vanish. The recent measurements on  $K^+\Lambda$  production [13] clearly show this asymmetry approaching +1 at 0 degrees, along with MAID predictions approaching -1.

The trends in  $C_{x'}$  and  $C_{z'}$  for  $\gamma p \rightarrow K^+\Lambda$  are illustrated with two energies in Fig. 3. The data (green circles) are recent CLAS results from [13] and these are compared to the direct predictions from Kaon-MAID (blue-dashed curves) and K-SAID (black dotted curves) codes. For  $C_{z'}$  these clearly have the wrong limits at 0 and 180 degrees. Also shown are predictions using the multipoles from [20] passed through our above expressions to construct observables (solid red curves). The difference in signs is also evident in  $C_{x'}$ , particularly at low energies where only a few partial waves are contributing - top panels of Fig. 3. There it is clear that the predictions of the different partial solutions are essentially very similar, differing only in sign.

Finally, we note that when fitting amplitudes from large numbers of measurements of different observables it will be important to evaluate and treat systematic uncertainties

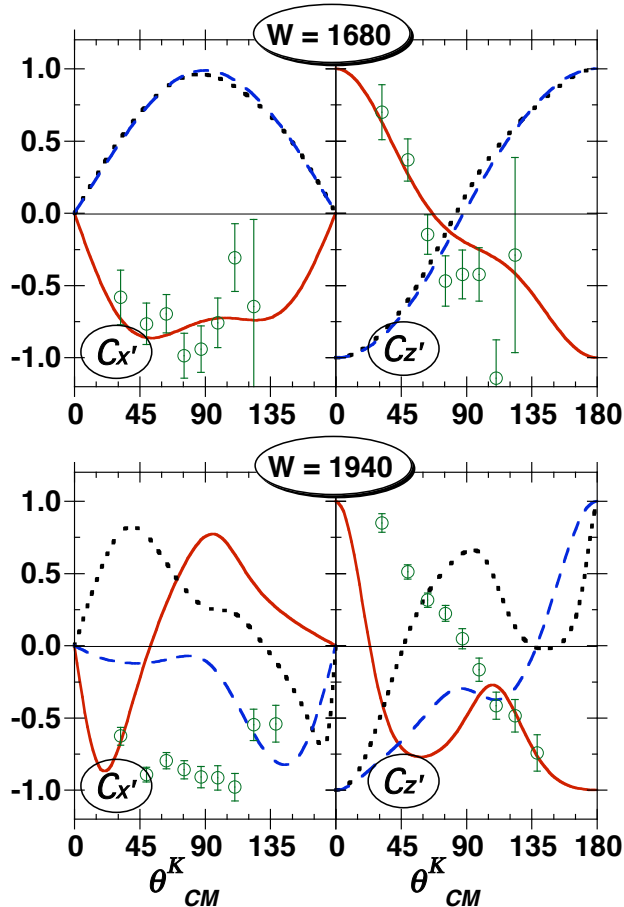


FIG. 3:  $C_{x'}$  (left) and  $C_{z'}$  (right) for the  $\gamma p \rightarrow K^+ \Lambda$  reaction at  $W = 1680$  MeV (top) and  $W = 1940$  MeV (bottom). Kaon-MAID predictions are dashed [15–17], K-SAID predictions are dotted [18, 19]. Predictions using the multipoles of [20] and our equations are shown as solid red curves. The green circles are from [13].

in a consistent manner. Here the Fierz relations will be particularly useful, allowing the comparison of data on one observable with an evaluation in terms of products of other observables. We have numerically checked the 37 Fierz identities of ref. [1]. A revised set with corrected signs is listed in Appendix B.

In summary, we have explicitly listed the experimental measurements needed to construct all of the 16 spin observables in pseudoscalar photo-production and provided a consistent set of equations relating these quantities to the CGLN amplitudes, and from these to the multipoles. Comparing to previous works, we have found that the combinations of measurements implied by the six  $H$ ,  $L_{x'}$ ,  $C_{x'}$ ,  $C_{z'}$ ,  $O_{x'}$  and  $O_{z'}$  observables calculated in MAID (and we assume in SAID as well) appears to be the negative of what is in common use by experi-

mental groups [13, 21]. Neglecting this when fitting amplitudes from complete experiments would drastically alter the resultant multipoles.

### **Acknowledgments**

This work was supported by the U.S. Department of Energy, Office of Nuclear Physics Division, under Contract No. DE-AC05-060R23177 under which Jefferson Science Associates operates Jefferson Laboratory, and also by the U.S. Department of Energy, Office of Nuclear Physics Division, under Contract No. DE-AC02-06CH11357 and Contract No. DE-FG02-97ER41025.

### **Appendix A: Constructing Observables from Measurements**

We tabulate here the pairs of measurements needed to construct each of the 16 transverse photo-production observables in terms of the polarization orientation angles of Fig. 2. The photon beam is characterized either by its helicity,  $h_\gamma$  for circular polarization, or by  $\phi_\gamma^L$  for linear polarization. Assuming 100% polarizations, each observable  $\hat{A} = A\sigma_0$  is determined by a pair of measurements, each denoted as  $\sigma(B, T, R)$ ; “*unp*” indicates the need to average over the initial spin states of the target or beam, and to sum over the final spin states of the recoil baryon. For observables involving only beam or target polarizations,  $\hat{A} = (1/2)(\sigma_1 - \sigma_2)$ . For observables involving the final state recoil polarization,  $\hat{A} = (\sigma_1 - \sigma_2)$ .

TABLE II: The cross section and observables involving only one polarization.

$\Sigma, T, P$		Beam		Target		Recoil	
Observable	$(\sigma_1, \sigma_2)$	$h_\gamma$	$\phi_\gamma^L$	$\theta_p$	$\phi_p$	$\theta_{p'}$	$\phi_{p'}$
$\sigma_0$		<i>unp</i>	<i>unp</i>	<i>unp</i>	<i>unp</i>	<i>unp</i>	<i>unp</i>
$\hat{\Sigma}$	$\sigma_1 = \sigma(\perp, 0, 0)$	-	$\pi/2$	<i>unp</i>	<i>unp</i>	<i>unp</i>	<i>unp</i>
	$\sigma_2 = \sigma(\parallel, 0, 0)$	-	0	<i>unp</i>	<i>unp</i>	<i>unp</i>	<i>unp</i>
$\hat{T}$	$\sigma_1 = \sigma(0, +y, 0)$	<i>unp</i>	<i>unp</i>	$\pi/2$	$\pi/2$	<i>unp</i>	<i>unp</i>
	$\sigma_2 = \sigma(0, -y, 0)$	<i>unp</i>	<i>unp</i>	$\pi/2$	$3\pi/2$	<i>unp</i>	<i>unp</i>
$\hat{P}$	$\sigma_1 = \sigma(0, 0, +y')$	<i>unp</i>	<i>unp</i>	<i>unp</i>	<i>unp</i>	$\pi/2$	$\pi/2$
	$\sigma_2 = \sigma(0, 0, -y')$	<i>unp</i>	<i>unp</i>	<i>unp</i>	<i>unp</i>	$\pi/2$	$3\pi/2$

TABLE III: Observables involving both beam and target polarization.

$B - T$		Beam		Target		Recoil	
Observable	$(\sigma_1, \sigma_2)$	$h_\gamma$	$\phi_\gamma^L$	$\theta_p$	$\phi_p$	$\theta_{p'}$	$\phi_{p'}$
$\hat{E}$	$\sigma_1 = \sigma(+1, -z, 0)$	+1	-	$\pi$	0	<i>unp</i>	<i>unp</i>
	$\sigma_2 = \sigma(+1, +z, 0)$	+1	-	0	0	<i>unp</i>	<i>unp</i>
$\hat{E}$	$\sigma_1 = \sigma(+1, -z, 0)$	+1	-	$\pi$	0	<i>unp</i>	<i>unp</i>
	$\sigma_2 = \sigma(-1, -z, 0)$	-1	-	$\pi$	0	<i>unp</i>	<i>unp</i>
$\hat{G}$	$\sigma_1 = \sigma(+\pi/4, +z, 0)$	-	$\pi/4$	0	0	<i>unp</i>	<i>unp</i>
	$\sigma_2 = \sigma(+\pi/4, -z, 0)$	-	$\pi/4$	$\pi$	0	<i>unp</i>	<i>unp</i>
$\hat{G}$	$\sigma_1 = \sigma(+\pi/4, +z, 0)$	-	$\pi/4$	0	0	<i>unp</i>	<i>unp</i>
	$\sigma_2 = \sigma(-\pi/4, +z, 0)$	-	$3\pi/4$	0	0	<i>unp</i>	<i>unp</i>
$\hat{F}$	$\sigma_1 = \sigma(+1, +x, 0)$	+1	-	$\pi/2$	0	<i>unp</i>	<i>unp</i>
	$\sigma_2 = \sigma(-1, +x, 0)$	-1	-	$\pi/2$	0	<i>unp</i>	<i>unp</i>
$\hat{F}$	$\sigma_1 = \sigma(+1, +x, 0)$	+1	-	$\pi/2$	0	<i>unp</i>	<i>unp</i>
	$\sigma_2 = \sigma(+1, -x, 0)$	+1	-	$\pi/2$	$\pi$	<i>unp</i>	<i>unp</i>
$\hat{H}$	$\sigma_1 = \sigma(+\pi/4, +x, 0)$	-	$\pi/4$	$\pi/2$	0	<i>unp</i>	<i>unp</i>
	$\sigma_2 = \sigma(-\pi/4, +x, 0)$	-	$3\pi/4$	$\pi/2$	0	<i>unp</i>	<i>unp</i>
$\hat{H}$	$\sigma_1 = \sigma(+\pi/4, +x, 0)$	-	$\pi/4$	$\pi/2$	0	<i>unp</i>	<i>unp</i>
	$\sigma_2 = \sigma(+\pi/4, -x, 0)$	-	$\pi/4$	$\pi/2$	$\pi$	<i>unp</i>	<i>unp</i>

TABLE IV: Observables involving both beam and recoil polarization.

$B - R$		Beam		Target		Recoil	
Observable	$(\sigma_1, \sigma_2)$	$h_\gamma$	$\phi_\gamma^L$	$\theta_p$	$\phi_p$	$\theta_{p'}$	$\phi_{p'}$
$\hat{C}_{x'}$	$\sigma_1 = \sigma(+1, 0, +x')$	+1	-	<i>unp</i>	<i>unp</i>	$\pi/2 + \theta_K$	0
	$\sigma_2 = \sigma(-1, 0, +x')$	-1	-	<i>unp</i>	<i>unp</i>	$\pi/2 + \theta_K$	0
$\hat{C}_{x'}$	$\sigma_1 = \sigma(+1, 0, +x')$	+1	-	<i>unp</i>	<i>unp</i>	$\pi/2 + \theta_K$	0
	$\sigma_2 = \sigma(+1, 0, -x')$	+1	-	<i>unp</i>	<i>unp</i>	$3\pi/2 + \theta_K$	0
$\hat{C}_{z'}$	$\sigma_1 = \sigma(+1, 0, +z')$	+1	-	<i>unp</i>	<i>unp</i>	$\theta_K$	0
	$\sigma_2 = \sigma(-1, 0, +z')$	-1	-	<i>unp</i>	<i>unp</i>	$\theta_K$	0
$\hat{C}_{z'}$	$\sigma_1 = \sigma(+1, 0, +z')$	+1	-	<i>unp</i>	<i>unp</i>	$\theta_K$	0
	$\sigma_2 = \sigma(+1, 0, -z')$	+1	-	<i>unp</i>	<i>unp</i>	$\pi + \theta_K$	0
$\hat{O}_{x'}$	$\sigma_1 = \sigma(+\pi/4, 0, +x')$	-	$\pi/4$	<i>unp</i>	<i>unp</i>	$\pi/2 + \theta_K$	0
	$\sigma_2 = \sigma(-\pi/4, 0, +x')$	-	$3\pi/4$	<i>unp</i>	<i>unp</i>	$\pi/2 + \theta_K$	0
$\hat{O}_{x'}$	$\sigma_1 = \sigma(+\pi/4, 0, +x')$	-	$\pi/4$	<i>unp</i>	<i>unp</i>	$\pi/2 + \theta_K$	0
	$\sigma_2 = \sigma(+\pi/4, 0, -x')$	-	$\pi/4$	<i>unp</i>	<i>unp</i>	$3\pi/2 + \theta_K$	0
$\hat{O}_{z'}$	$\sigma_1 = \sigma(+\pi/4, 0, +z')$	-	$\pi/4$	<i>unp</i>	<i>unp</i>	$\theta_K$	0
	$\sigma_2 = \sigma(-\pi/4, 0, +z')$	-	$3\pi/4$	<i>unp</i>	<i>unp</i>	$\theta_K$	0
$\hat{O}_{z'}$	$\sigma_1 = \sigma(+\pi/4, 0, +z')$	-	$\pi/4$	<i>unp</i>	<i>unp</i>	$\theta_K$	0
	$\sigma_2 = \sigma(+\pi/4, 0, -z')$	-	$\pi/4$	<i>unp</i>	<i>unp</i>	$\pi + \theta_K$	0

TABLE V: Observables involving both target and recoil polarization.

$T - R$		Beam		Target		Recoil	
Observable	$(\sigma_1, \sigma_2)$	$h_\gamma$	$\phi_\gamma^L$	$\theta_p$	$\phi_p$	$\theta_{p'}$	$\phi_{p'}$
$\hat{L}_{x'}$	$\sigma_1 = \sigma(0, +z, +x')$	<i>unp</i>	<i>unp</i>	0	0	$\pi/2 + \theta_K$	0
	$\sigma_2 = \sigma(0, -z, +x')$	<i>unp</i>	<i>unp</i>	$\pi$	0	$\pi/2 + \theta_K$	0
$\hat{L}_{x'}$	$\sigma_1 = \sigma(0, +z, +x')$	<i>unp</i>	<i>unp</i>	0	0	$\pi/2 + \theta_K$	0
	$\sigma_2 = \sigma(0, +z, -x')$	<i>unp</i>	<i>unp</i>	0	0	$3\pi/2 + \theta_K$	0
$\hat{L}_{z'}$	$\sigma_1 = \sigma(0, +z, +z')$	<i>unp</i>	<i>unp</i>	0	0	$\theta_K$	0
	$\sigma_2 = \sigma(0, -z, +z')$	<i>unp</i>	<i>unp</i>	$\pi$	0	$\theta_K$	0
$\hat{L}_{z'}$	$\sigma_1 = \sigma(0, +z, +z')$	<i>unp</i>	<i>unp</i>	0	0	$\theta_K$	0
	$\sigma_2 = \sigma(0, +z, -z')$	<i>unp</i>	<i>unp</i>	0	0	$\pi + \theta_K$	0
$\hat{T}_{x'}$	$\sigma_1 = \sigma(0, +x, +x')$	<i>unp</i>	<i>unp</i>	$\pi/2$	0	$\pi/2 + \theta_K$	0
	$\sigma_2 = \sigma(0, -x, +x')$	<i>unp</i>	<i>unp</i>	$\pi/2$	$\pi$	$\pi/2 + \theta_K$	0
$\hat{T}_{x'}$	$\sigma_1 = \sigma(0, +x, +x')$	<i>unp</i>	<i>unp</i>	$\pi/2$	0	$\pi/2 + \theta_K$	0
	$\sigma_2 = \sigma(0, +x, -x')$	<i>unp</i>	<i>unp</i>	$\pi/2$	0	$3\pi/2 + \theta_K$	0
$\hat{T}_{z'}$	$\sigma_1 = \sigma(0, +x, +z')$	<i>unp</i>	<i>unp</i>	$\pi/2$	0	$\theta_K$	0
	$\sigma_2 = \sigma(0, -x, +z')$	<i>unp</i>	<i>unp</i>	$\pi/2$	$\pi$	$\theta_K$	0
$\hat{T}_{z'}$	$\sigma_1 = \sigma(0, +x, +z')$	<i>unp</i>	<i>unp</i>	$\pi/2$	0	$\theta_K$	0
	$\sigma_2 = \sigma(0, +x, -z')$	<i>unp</i>	<i>unp</i>	$\pi/2$	0	$\pi + \theta_K$	0

## Appendix B: The Fierz Identities

We list here the Fierz identities relating *asymmetries*, with corrected signs. The equation numbering sequence is that of Chiang and Tabakin [1]. Compared to the latter, signs have changed in all but (L.1), (L.4-6), (Q.r), (Q.bt.3), (Q.tr.1-2), and of course the six *Squared* relations. Sign changes in eight of the equations can be attributed to the different definition for the  $E$  asymmetry used by Fasano, Tabakin and Saghai [9], to which Chiang and Tabakin refer. (We note that sign changes in another 15 equations could have been explained if the definition of the beam asymmetry ( $\Sigma$ ) were also reversed; but our definition of  $\Sigma$  in Table A1 is identical to that of Fasano, Tabakin and Saghai [9].)

### 1. Linear-Quadratic relations

$$1 = \{\Sigma^2 + T^2 + P^2 + E^2 + G^2 + F^2 + H^2 + O_{x'}^2 + O_{z'}^2 + C_{x'}^2 + C_{z'}^2 + L_{x'}^2 + L_{z'}^2 + T_{x'}^2 + T_{z'}^2\}/3 \quad (\text{L.0})$$

$$\Sigma = +TP + T_{x'}L_{z'} - T_{z'}L_{x'} \quad (\text{L.TR})$$

$$T = +\Sigma P - C_{x'}O_{z'} + C_{z'}O_{x'} \quad (\text{L.BR})$$

$$P = +\Sigma T + GF + EH \quad (\text{L.BT})$$

$$G = +PF + O_{x'}L_{x'} + O_{z'}L_{z'} \quad (\text{L.1})$$

$$H = +PE + O_{x'}T_{x'} + O_{z'}T_{z'} \quad (\text{L.2})$$

$$E = +PH - C_{x'}L_{x'} - C_{z'}L_{z'} \quad (\text{L.3})$$

$$F = +PG + C_{x'}T_{x'} + C_{z'}T_{z'} \quad (\text{L.4})$$

$$O_{x'} = +TC_{z'} + GL_{x'} + HT_{x'} \quad (\text{L.5})$$

$$O_{z'} = -TC_{x'} + GL_{z'} + HT_{z'} \quad (\text{L.6})$$

$$C_{x'} = -TO_{z'} - EL_{x'} + FT_{x'} \quad (\text{L.7})$$

$$C_{z'} = +TO_{x'} - EL_{z'} + FT_{z'} \quad (\text{L.8})$$

$$T_{x'} = +\Sigma L_{z'} + HO_{x'} + FC_{x'} \quad (\text{L.9})$$

$$T_{z'} = -\Sigma L_{x'} + HO_{z'} + FC_{z'} \quad (\text{L.10})$$

$$L_{x'} = -\Sigma T_{z'} + GO_{x'} - EC_{x'} \quad (\text{L.11})$$

$$L_{z'} = +\Sigma T_{x'} + GO_{z'} - EC_{z'} \quad (\text{L.12})$$

## 2. Quadratic relations

$$C_{x'}O_{x'} + C_{z'}O_{z'} + EG - FH = 0 \quad (\text{Q.b})$$

$$GH - EF - L_{x'}T_{x'} - L_{z'}T_{z'} = 0 \quad (\text{Q.t})$$

$$C_{x'}C_{z'} + O_{x'}O_{z'} - L_{x'}L_{z'} - T_{x'}T_{z'} = 0 \quad (\text{Q.r})$$

$$\Sigma G - TF - O_{z'}T_{x'} + O_{x'}T_{z'} = 0 \quad (\text{Q.bt.1})$$

$$\Sigma H - TE + O_{z'}L_{x'} - O_{x'}L_{z'} = 0 \quad (\text{Q.bt.2})$$

$$\Sigma E - TH + C_{z'}T_{x'} - C_{x'}T_{z'} = 0 \quad (\text{Q.bt.3})$$

$$\Sigma F - TG + C_{z'}L_{x'} - C_{x'}L_{z'} = 0 \quad (\text{Q.bt.4})$$

$$\Sigma O_{x'} - PC_{z'} + GT_{z'} - HL_{z'} = 0 \quad (\text{Q.br.1})$$

$$\Sigma O_{z'} + PC_{x'} - GT_{x'} + HL_{x'} = 0 \quad (\text{Q.br.2})$$

$$\Sigma C_{x'} + PO_{z'} - ET_{z'} - FL_{z'} = 0 \quad (\text{Q.br.3})$$

$$\Sigma C_{z'} - PO_{x'} + ET_{x'} + FL_{x'} = 0 \quad (\text{Q.br.4})$$

$$TT_{x'} - PL_{z'} - HC_{z'} + FO_{z'} = 0 \quad (\text{Q.tr.1})$$

$$TT_{z'} + PL_{x'} + HC_{x'} - FO_{x'} = 0 \quad (\text{Q.tr.2})$$

$$TL_{x'} + PT_{z'} - GC_{z'} - EO_{z'} = 0 \quad (\text{Q.tr.3})$$

$$TL_{z'} - PT_{x'} + GC_{x'} + EO_{x'} = 0 \quad (\text{Q.tr.4})$$

### 3. Squared relations

$$G^2 + H^2 + E^2 + F^2 + \Sigma^2 + T^2 - P^2 = 1 \quad (\text{S.bt})$$

$$O_{x'}^2 + O_{z'}^2 + C_{x'}^2 + C_{z'}^2 + \Sigma^2 - T^2 + P^2 = 1 \quad (\text{S.br})$$

$$T_{x'}^2 + T_{z'}^2 + L_{x'}^2 + L_{z'}^2 - \Sigma^2 + T^2 + P^2 = 1 \quad (\text{S.tr})$$

$$G^2 + H^2 - E^2 - F^2 - O_{x'}^2 - O_{z'}^2 + C_{x'}^2 + C_{z'}^2 = 0 \quad (\text{S.b})$$

$$G^2 - H^2 + E^2 - F^2 + T_{x'}^2 + T_{z'}^2 - L_{x'}^2 - L_{z'}^2 = 0 \quad (\text{S.t})$$

$$O_{x'}^2 - O_{z'}^2 + C_{x'}^2 - C_{z'}^2 - T_{x'}^2 + T_{z'}^2 - L_{x'}^2 + L_{z'}^2 = 0 \quad (\text{S.r})$$

- [1] W.-T. Chaing and F. Tabakin, Phys. Rev. C **55**, 2054 (1997).
- [2] *The g9-frost series of experiments*, URL <http://clasweb.jlab.org/shift/g9/>.
- [3] *The g14-HDice experiment*, URL [http://www.jlab.org/exp\\_prog/proposals/06/PR-06-101.pdf](http://www.jlab.org/exp_prog/proposals/06/PR-06-101.pdf).
- [4] G. F. Chew et al., Phys. Rev. **105**, 1345 (1957).
- [5] I. S. Barker et al., Nucl. Phys. B **95**, 347 (1975).
- [6] A. Donnachie and G. Shaw, Appl. Phys. **37**, 333 (1966).
- [7] A. Donnachie, Pure and Applied Physics **25-V**, 1 (1972), ed. E.H.S. Bishop, Academic Press, NY.
- [8] R. A. Adelseck and B. Saghai, Phys. Rev. C **42**, 108 (1990).
- [9] C. G. Fasano, F. Tabakin, and B. Saghai, Phys. Rev. C **46**, 2430 (1992).
- [10] D. Drechsel and L. Tiator, J. Phys. G: Nucl. Part. Phys. **18**, 449 (1992).
- [11] G. Knochlein, D. Drechsel, and L. Tiator, Z. Phys. A **352**, 327 (1995).
- [12] J. D. Jackson, *Classical Electrodynamics* (John Wiley & Sons, NY, 1975).
- [13] CLAS Collaboration, R. K. Bradford, et al., Phys. Rev. C **75**, 035205 (2007).
- [14] J. D. Bjorken and S. D. Drell, *Relativistic Quantum Mechanics* (McGraw-Hill, New York, 1964).
- [15] *MAID and Kaon-MAID isobar models of meson production*, URL <http://wwwkph.kph.uni-mainz.de/MAID/>.
- [16] D. Drechsel, S. S. Kamalov, and L. Tiator, Eur. Phys. J. A **34**, 69 (2007).

- [17] T. Mart and C. Benhold, Phys. Rev. C **66**, 012201 (2000).
- [18] *SAID partial wave analysis facility*, URL <http://gwdac.phys.gwu.edu/>.
- [19] R. A. Arndt et al., Phys. Rev. C **66**, 055213 (2002).
- [20] B. Juliá-Díaz et al., Phys. Rev. C **73**, 055204 (2006).
- [21] C. A. Paterson, Ph.D. thesis, University of Glasgow (2008), CLAS Collaboration, analysis of g8 data.